THE JOURNAL OF PHYSICAL CHEMISTRY C

Article

pubs.acs.org/JPCC

# Dynamics of Molecular Monolayers with Different Chain Lengths in Air and Solvents Probed by Ultrafast 2D IR Spectroscopy

Jun Nishida, Chang Yan, and Michael D. Fayer*

Department of Chemistry, Stanford University, Stanford, California 94305, United States

**ABSTRACT:** The ultrafast dynamics of functionalized alkylsilane monolayers with two different alkyl chain lengths, $C_{11}$ and $C_3$, are studied by 2D IR vibrational echo spectroscopy. Terminal sites of the monolayers are functionalized with an IR probe, tricarbonyl (1,10-phenanthroline) rhenium chloride ($RePhen(CO)_3Cl$), to report on the structural dynamics of monolayer-air and monolayer-solvent interfaces. Frequency−frequency correlation functions (FFCF) of symmetric CO stretching mode were extracted from 2D IR spectra. The FFCF provides information on the time evolution of surface structures that contribute to the inhomogeneously broadened IR absorption spectrum of the CO stretch by quantifying spectral diffusion. To elucidate the detailed structural dynamics with accurate time constants, FFCF decays were monitored to 60 ps, a major improvement over prior experiments. Without the presence of solvents, $C_3$ monolayers have significantly slower spectral diffusion (66 ps) than $C_{11}$ monolayer (38 ps). This difference supports the previous postulate that spectral diffusion associated with the molecular monolayer in air involves the structural dynamics of the tethering alkyl chains. With the $C_{11}$ and $C_3$ monolayers immersed in dimethylformamide (DMF), in which $RePhen(CO)_3Cl$ is soluble, the FFCFs of both samples display biexponential decays with the time constants of 5.6 and 43 ps for $C_{11}$ and 5.9 and 63 ps for $C_3$. The slower time constants are in good agreement with the spectral diffusion time constants observed in the absence of solvent, indicating that these slower components still reflect the monolayers' dynamics, which are not affected by the presence of the solvent. Because the faster time constants were independent of chain length and similar to that of the $RePhen(CO)_3Cl$ headgroup in bulk DMF solution, they are attributed to the dynamics of the interfacial DMF molecules. When monolayers were immersed in hexadecane, in which $RePhen(CO)_3Cl$ is not soluble, slower dynamics were again observed for the $C_3$ monolayer than the $C_{11}$ monolayer. The orientational dynamics of the IR probes were studied using polarization selective heterodyne detected transient grating experiments as well.

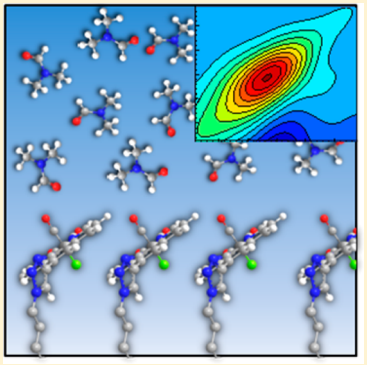

## I. INTRODUCTION

Surface functionalized organic monolayers are of considerable interests due to their possible applications in molecular heterogeneous catalysts,[1−4] photovoltaic cells,[5] chemical and biological sensors,[6−8] and electrochemical switching of surface properties.[9] There are a large number of sophisticated methods for characterizing molecular monolayers such as linear infrared spectroscopy,[10] electron-energy loss spectroscopy,[11] sum-frequency generation spectroscopy,[12] X-ray photoelectron spectroscopy,[13] atomic force microscopy,[14,15] and scanning tunneling microscopy.[16] Sum frequency generation (SFG) spectroscopy has been successful in selectively providing detailed structural information on interfacial molecules, such as the orientations on interfaces[17,18] and conformations of alkyl chains tethered to surfaces.[19,20] None of these methods, however, can address surface molecular dynamics on the time scales of molecular motions.

Investigation of interfacial molecular dynamics requires techniques that can both operate on ultrafast time scales and selectively extract signals from interfaces without being overwhelmed by signals from the bulk medium. Time-resolved SFG methods can extract orientational dynamics information on interfaces,[21−24] although the interpretation of the data can be complex.[25] Two-dimensional infrared (2D IR) spectroscopy has proven to be a powerful tool to probe the dynamics of molecules in condensed phases, such as the dynamics of water in various environments,[26−32] dynamical solute−solvent interactions,[33−36] and ultrafast structural evolution in proteins.[37−39] One of the promising approaches for the study of interfacial molecular dynamics is to combine SFG with nonlinear IR spectroscopy.[40] Following the earliest successful work on SFG-two pulse echoes experiments by Guyot-Sionnest and co-workers,[41,42] surface selective SFG-2D IR spectroscopies have been reported recently.[43−47]

We have taken another approach to study interfacial molecular dynamics by chemically immobilizing the functional group tricarbonyl (1,10-phenanthroline) rhenium chloride ($RePhen(CO)_3Cl$) on surfaces. $SiO_2$ surfaces are functionalized with alkylsilane monolayers with the $RePhen(CO)_3Cl$ as the head groups on the alkyl chains. We then directly apply 2D IR heterodyne detected vibrational echo spectroscopy to the functionalized monolayers using the tricarbonyl symmetric stretching mode as the IR probe.[48] The symmetric CO stretching mode of $RePhen(CO)_3Cl$ has a large transition

**Received:** October 29, 2013
**Revised:** December 15, 2013
**Published:** December 19, 2013

  

dipole (integrated extinction coefficient of $3 \times 10^7$ O.D./(mol $cm^{-2}$)) and a reasonably long vibrational lifetime, ~20 ps. Because of these properties of the IR probe, we are able to obtain useful 2D IR spectra to track the dynamics of the monolayer over a significant time range without the additional step of sum frequency generation upconversion.

We have successfully applied this approach to observe the spectral diffusion of symmetric CO stretching mode for monolayer−air and monolayer−solvent interfaces.[49,50] Spectral diffusion is caused by motions of the molecular system that change the local environments of molecules and therefore change the vibrational frequency. Therefore, spectral diffusion is directly related to the structural evolution of the system. In spite of the fact that a monolayer contains very few molecules, increased IR pulse energy and long-term system stability, enabling signal averaging of multiple measurements over several days, made it possible to observe the spectral diffusion dynamics to 60 ps with much better accuracy compared to previous experiments on this type of system.[48−50]

In the present study, we address the spectral diffusion mechanism for both monolayer−air and monolayer−solvent interfaces by studying the dependence of the spectral diffusion rates on the length of tethering alkyl chains. Two types of monolayers, comprised of undecyl ($C_{11}$) and propyl ($C_3$) alkyl chains, are studied and compared for various interfaces, i.e., monolayer−air, monolayer−dimethylformamide (DMF), and monolayer−hexadecane interfaces. DMF was chosen as a representative of polar solvents that dissolve the IR probe, $RePhen(CO)_3Cl$, but is not miscible with alkanes. Hexadecane was chosen as a nonpolar solvent in which the IR probe is insoluble but is miscible with alkanes. The results presented below show that the spectral diffusion rates are significantly different for $C_{11}$ and $C_3$ monolayers with air interfaces. For these systems, there are no solvent dynamics involved. Therefore, the spectral diffusion is caused by structural dynamics of monolayer's alkyl chains, linker, and headgroup. A careful investigation of spectral diffusion for the monolayer-DMF interfaces shows that the decays have biexponential forms. The results indicate that a fast component of the spectral diffusion is caused by the DMF dynamics at the interface, while the slow component is caused by the motions of the surface bound molecules. For the monolayer in hexadecane, the results are not as clear-cut, but the analysis suggests that there are solvent- and surface-bound molecule components in the observed dynamics as well.

In addition to measurements of spectral diffusion, we have also made measurements of the time dependence of the orientational anisotropy (orientational relaxation) using polarization selective heterodyne detected transient grating (HDTG) experiments. HDTG experiments provide essentially the same information as pump−probe experiment but with much greater sensitivity.[48−50] The results show that there are restricted motions over a range of angles, and the complete orientational randomization is not achieved. This type of motion is generally referred to as wobbling-in-a-cone.[51−54] The HDTG experiments were also used to determine the vibrational lifetimes.

## II. EXPERIMENTAL PROCEDURES

**A. Preparation of Functionalized Alkylsilane Monolayer.** The details for the preparation of functionalized $C_{11}$ or $C_3$ monolayer on $SiO_2$ surfaces were described previously.[48] One hundred nanometer silica layers were deposited on 3 mm thick calcium fluoride substrates with plasma enhanced chemical vapor deposition (PECVD). The $SiO_2/CaF_2$ wafers were incubated for 1 h in 1 ppm solution of 11-bromo-undecyltrichlorosilane or 3-bromo-propyltrichlorosilane in bicyclohexyl at room temperature to form $Br-C_{11}$ or $Br-C_3$ monolayers. The wafers were then immersed in saturated $NaN_3$ solution in DMF for 24 h to substitute the terminal bromine with azide by an $S_N2$ reaction, yielding $N_3-C_{11}$ or $N_3-C_3$ monolayers. Then, the terminal azide group was used for copper catalyzed azide−alkyne cycloaddition (CuAAC) with *fac*-$Re(phenC{\equiv}CH)(CO)_3Cl$ to covalently attach the IR probe to the monolayers of alkyl chains.

**B. 2D IR Spectroscopy.** The 100 fs IR pulse (5.5−6 $\mu$J, peaked at 2025 $cm^{-1}$ with ~90 $cm^{-1}$ full width at half-maximum (fwhm)) was split into four pulses, and three of the pulses were used for the creation of vibrational echo signal and the other weak pulse served as a local oscillator (LO). The three pulses (pulses 1, 2, 3 in temporal order) are crossed on the monolayer deposited on a $CaF_2$-on-$SiO_2$ wafer in BOXCARS geometry. The generated echo pulse was spatially and temporarily overlapped with a local oscillator pulse and sent to a monochromator. The spectrally dispersed signal is detected by 32-pixel MCT array. The array frequencies ($\omega_m$) are the vertical axis of the 2D IR spectra. The horizontal axis of the 2D spectra, $\omega_\tau$, is obtained by Fourier transform of temporal interferogram on each $\omega_m$ pixel obtained by scanning the delay $\tau$ between pulses 1 and 2.

2D IR spectra are generated for each waiting time $T_w$ (the delay between pulses 2 and 3) using the appropriate data processing.[55] At very short $T_w$, the 2D spectrum will be elongated along the diagonal due to strong correlation between $\omega_\tau$ and $\omega_m$. As $T_w$ increases, the spectrum will become increasingly round. By estimating the center line slope (CLS) of each band in 2D spectrum, together with the absorption line width, the frequency−frequency correlation function (FFCF) can be extracted.[56,57] The FFCF was modeled with a multiexponential form

$$C(t) = \langle \delta\omega_{1,0}(\tau_1)\delta\omega_{1,0}(0)\rangle = \sum_i \Delta_i^2 \exp(-t/\tau_i) \quad (1)$$

where the $\Delta_i$ are the frequency fluctuation amplitudes of each component, and the $\tau_i$ are their associated time constants. A component of the FFCF with $\Delta\tau < 1$ is motionally narrowed, and it is a source of the homogeneous broadening of the absorption line. When a component of the dynamics is motionally narrowed, $\Delta$ and $\tau$ cannot be determined separately. The motionally narrowed homogeneous contribution to the absorption spectrum has a pure dephasing line width given by $\Gamma^* = \Delta^2\tau = 1/\pi T_2^*$, where $T_2^*$ is the pure dephasing time. The observed homogeneous dephasing time, $T_2$, also has contributions from the vibrational lifetime and orientational relaxation:

$$\frac{1}{T_2} = \frac{1}{T_2^*} + \frac{1}{2T_1} + \frac{1}{3T_{or}} \quad (2)$$

where $T_1$ and $T_{or}$ are the vibrational lifetime and orientational relaxation time, respectively. The total homogeneous line width is $\Gamma = 1/\pi T_2$. As discussed below, the vibrational lifetimes, $T_1$, are all about 20 ps, so the lifetime contribution to the homogeneous line width is ~0.25 $cm^{-1}$. There is some degree of incomplete orientational relaxation (see below), which will also make a small contribution to the homogeneous line width.


dx.doi.org/10.1021/jp410683h | J. Phys. Chem. C 2014, 118, 523−532

Since lifetime and orientational relaxation contributions are small, the homogeneous line width is dominated by the pure dephasing, $T_2^*$.

**C. Polarization Selective HDTG Spectroscopy.** Polarization selective HDTG spectroscopy was implemented using the same setup as 2D IR spectroscopy by temporally overlapping pulses 1 and 2. Details of the method have been presented previously.[48,49] Sets of $\lambda/2$ plate and polarizer were installed in the optical path of beams 1 and 2, so that the polarizations of these beams can be set either to $X$ or $Y$. The polarizations of beam 3 and the LO were fixed to $X$. Our previous report on polarization selective HDTG experiment was limited to the comparison of the time-dependent shapes of $I_{XXXX}$ (parallel polarization) and $I_{XXYY}$ (perpendicular polarization) signals,[49] where four subscripts indicate the polarizations of LO, pulse 3, pulse 2, and pulse 1. To obtain the anisotropy, it is necessary to measure $I_{XXXX} - I_{XXYY}$. Because of the difficulty of obtaining $I_{XXXX}$ and $I_{XXYY}$ with correct absolute amplitudes, the anisotropy was not successfully extracted in our previous experiments.[49]

To solve this problem, we measure the thermally induced grating signal from a $D_2O$ sample.[50] The important feature of the thermal induced grating is that it is isotropic. $I_{XXXX}$ and $I_{XXYY}$ would be identical if the two excitation conditions were identical.[58] Therefore, the measured ratio of $I_{XXXX}$ and $I_{XXYY}$ from the thermally induced gratings provides the necessary correction factor so that the anisotropy can be determined for the monolayer samples. From the isotropic thermally induced grating measurements of $D_2O$, it was found that the correction factor is given by $f = I_{\mathrm{therm},XXYY}/I_{\mathrm{therm},XXXX} = 0.76$. $I_{XXXX}$ data was multiplied by $f$, so the factor does not appear explicitly in the following discussion. The anisotropy $r(t)$ is obtained from the measurements of $I_{XXXX}$ and $I_{XXYY}$ as

$$r(t) = \frac{I_{XXXX} - I_{XXYY}}{I_{XXXX} + 2I_{XXYY}} \tag{3}$$

The denominator of eq 3 is defined as $P(t)$:

$$P(t) = I_{XXXX} + 2I_{XXYY} \tag{4}$$

In the case where transition dipole moments are randomly oriented in the sample, the anisotropy $r(t)$ in eq 3 is proportional to orientational correlation function, and $P(t)$ is proportional to isotropic population decay (vibrational lifetime).[58,59] However, in the case of the monolayers on the two-dimensional surfaces, the orientations of transition dipole moments were restricted. As discussed in Section III.C, the interpretations of eqs 3 and 4 differ from those for a bulk system with an isotropic distribution of transition dipole directions.

## III. RESULTS AND DISCUSSION

**A. Infrared Absorption Spectroscopy.** The FT-IR spectra of the symmetric CO stretching mode of the $RePhen(CO)_3Cl$ probe on $C_{11}$ monolayer−air and $C_3$ monolayer−air interfaces for a number of independently prepared samples are shown in Figure 1A and B. The averages for all of the samples of the peak positions and bandwidths are listed in Table 1. The samples have absorbances of <1 mOD. In spite of the variations, especially in the $C_3$ monolayer, some general trends can be seen. First, the $C_{11}$ monolayers have higher optical densities than $C_3$ monolayer (0.70 ± 0.03 mOD for $C_{11}$ and 0.45 ± 0.14 mOD for $C_3$). Also, the peak positions

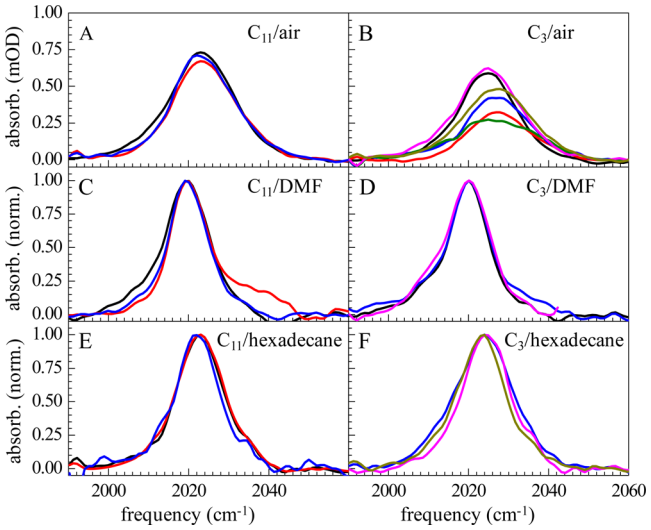


**Figure 1.** (A and B) Infrared absorption spectra of CO symmetric stretching mode of $RePhen(CO)_3Cl$ immobilized on the $C_{11}$ and $C_3$ monolayers in air. Three samples for $C_{11}$ monolayers and six samples for $C_3$ monolayers were measured and are plotted independently. The $C_3$ monolayer spectra show significant variance, and the peak positions are consistently bluer than $C_{11}$ monolayers. (C and D) Normalized absorption spectra of the same vibrational mode for monolayer/DMF interfaces. Three samples were measured for $C_{11}$ and $C_3$ monolayers. The bands are all centered at ~2020 $cm^{-1}$, regardless of the original peak positions on the monolayer/air interfaces. Narrower bandwidths are also evident. (E and F) Normalized absorption spectra for monolayer/hexadecane interfaces. Again, narrower bands than the monolayer/air interfaces are observed.

**Table 1. IR Absorption Peak Position and Full-Width-at-Half-Maximum for the Symmetric CO Stretching Mode of the IR Probe on the Various Interfaces**

| sample | chain length | peak position ($cm^{-1}$) | fwhm ($cm^{-1}$) |
|---|---|---|---|
| monolayer−air | $C_{11}$ | 2022.8 ± 0.6 | 18.0 ± 0.5 |
| | $C_3$ | 2025.9 ± 1.3 | 19.2 ± 2.9 |
| monolayer−DMF | $C_{11}$ | 2019.6 ± 0.2 | 11.7 ± 0.9 |
| | $C_3$ | 2020.1 ± 0.1 | 12.0 ± 0.9 |
| monolayer−hexadecane | $C_{11}$ | 2022.4 ± 0.7 | 13.3 ± 0.9 |
| | $C_3$ | 2024.1 ± 0.3 | 14.7 ± 1.5 |

are at higher frequencies for the $C_3$ monolayer (2025.9 ± 1.3 $cm^{-1}$) than for the $C_{11}$ monolayer (2022.8 ± 0.6 $cm^{-1}$). As seen in Figure 1B, as the peak height decreases, the peak position tends to shift to the blue (high frequency) in $C_3$ monolayers, indicating a possible correlation between the peak positions and the peak heights. Significant differences in the bandwidths were not observed within the error bars: 18.0 ± 0.5 $cm^{-1}$ fwhm for $C_{11}$ and 19.2 ± 2.9 $cm^{-1}$ fwhm for $C_3$.

Compared to the $C_{11}$ monolayers, the $C_3$ monolayers display significant variations in the peak positions, bandwidths, and peak heights, even though they are all synthesized with the same procedure. The irreproducibility of the formation of the alkylsilane monolayers has long been a standing issue, and it has been asserted that the silanization process is sensitive to the reaction conditions, especially temperature.[60] Brzoska et al. demonstrated that the complete formation of alkylsilane monolayers is achieved only when the temperature is lower than a certain critical temperature, which is dependent on the chain length.[61] As the chain length becomes shorter, this critical


dx.doi.org/10.1021/jp410683h | J. Phys. Chem. C 2014, 118, 523−532

temperature is lower. At room temperature, imperfect monolayers with defects are more likely to be formed. The existence of defects in the shorter-chain alkylsilane monolayers has been confirmed by the measurement of friction of grafted surfaces.[62] Since all the silanization steps for the monolayers shown in Figure 1A,B are performed at room temperature, it is reasonable that $C_3$ monolayers have less perfect structures than the $C_{11}$ monolayers, leading to less reproducible absorption bands. The reduced absorbance of the $C_3$ monolayers is likely to indicate fewer $C_3$ chains bound to the surface, considering that the average directions of the transition dipole moments were nearly the same between $C_{11}$ and $C_3$ monolayers.[49]

Figure 1C,D show the normalized FT-IR spectra of the $C_{11}$ and $C_3$ monolayers immersed in DMF. For both the $C_{11}$ can $C_3$ chain lengths, the peak positions shift to the red, and the linewidths become narrower (see Table 1). The change in linewidths is about the same for the two chain lengths, but the shift to lower frequency is larger for the $C_3$ chain length than for the $C_{11}$. Regardless of the monolayers' chain lengths, all the monolayers' absorption bands were centered at 2020 $cm^{-1}$ for the monolayer−DMF interfaces (2019.6 ± 0.2 $cm^{-1}$ for $C_{11}$ and 2020.0 ± 0.1 $cm^{-1}$ for $C_3$). This peak position is in excellent agreement with the symmetric CO stretching mode of the $RePhen(CO)_3Cl$ headgroup dissolved in bulk DMF solutions. These observations indicate that the IR probes are in close contact with the interfacial DMF molecules. The frequency shifts are caused by intermolecular interactions between DMF and the head groups. The averaged bandwidths on the monolayer−DMF interfaces were 11.7 ± 0.9 $cm^{-1}$ fwhm for $C_{11}$ and 12.0 ± 0.9 $cm^{-1}$ fwhm for $C_3$. Considering the previous observation that the bandwidth of the same vibrational mode of $RePhen(CO)_3Cl$ in the bulk DMF solution was 6.8 $cm^{-1}$,[50] the bandwidths on the monolayer−DMF interfaces lie between the bandwidths for bulk DMF solution and the bare monolayers without solvents. This result suggests that the FT-IR band shape of monolayer−DMF interface contains the information on both the configurations of interfacial DMF molecules and the alkyl chains of monolayers. This information is further extracted by the 2D IR experiment discussed in the next section.

Comparing panels B and D of Figure 1, an obvious change is that the distribution of peak positions and linewidths for the $C_3$/air spectra has vanished for $C_3$/DMF interfaces. Within experimental error, the $C_3$/DMF spectra have the same peak positions and widths. This is in contrast to the case of $C_{11}$ chains (Figures 1A,C), where for both $C_{11}$/air and $C_{11}$/DMF interfaces the spectra for the various samples do not show a significant distribution of peak positions and linewidths within experimental error. This different behavior observed by taking the monolayers from air to DMF indicates differences between the structure of the $C_{11}$ and $C_3$ monolayers.

During deposition of monolayers, the alkyl chains were attached to the silica surface by reactions between trichlorosilanes, surface Si−OH groups, and trace amount of adsorbed surface water. There is extensive literature showing that the reactions would lead to polymerization between different alkyl chains, forming Si−O−Si linkages among chains.[60,63,64] A network of alkyl chains is generated, and this network is attached to the surface at the SiOH sites. Therefore, the alkyl chains with their $RePhen(CO)_3Cl$ head groups are not bound directly to the surface, but rather project up from the network, which is attached to the surface. Presumably, the structure of this network is not as uniform as the $SiO_2$ surface, and also not completely reproducible from one synthesis to another. For the $C_{11}$ chains, the interaction among these long chains may overcome the disorder of the network and force a more uniform chain monolayer structure. By contrast, the short $C_3$ chains do not have nearly as many methylene−methylene interactions, resulting in insufficient chain−chain interactions to overcome the disorder of the underlying Si−O−Si network. The consequence would be a more disordered and less reproducible monolayer structure for the $C_3$ chains than the $C_{11}$ chains. A more disordered $C_3$ monolayer that varies from one synthetic preparation to another may produce more variation in the line width and peak position of IR probe compared to $C_{11}$ monolayers. When DMF is added, there are additional interactions between the $RePhen(CO)_3Cl$ head groups and the solvent. The variation of the peak position and line width for the $C_3$ monolayers may vanish due to this solvent-headgroup interaction. It is important to note that when the DMF was removed from the $C_3$ samples, the FT-IR spectra of the IR probe return to $C_3$/air spectra, suggesting that the underlying network disorder is not eliminated when the sample is immersed in DMF.

A similar behavior was observed when the $C_{11}$ and $C_3$ monolayers were immersed in hexadecane, although the spectral changes are less prominent than those caused by immersion in DMF. On average, the peak positions were 2022.4 ± 0.7 $cm^{-1}$ for $C_{11}$ monolayers and 2024.1 ± 0.3 $cm^{-1}$ for $C_3$ monolayers, which are slightly red-shifted compared to the peak positions for the monolayer-air interfaces. Narrower linewidths were observed for both the $C_{11}$ (13.3 ± 0.9 $cm^{-1}$) and $C_3$ (14.7 ± 1.5 $cm^{-1}$) monolayer−hexadecane interfaces. Since $RePhen(CO)_3Cl$ is not soluble in hexadecane, the comparison with the absorption band in bulk solution cannot be made. While the peak positions of monolayer−DMF interfaces were essentially the same for the $C_{11}$ and $C_3$ monolayers, there is a significant difference in the peak positions of the $C_{11}$ and $C_3$ monolayers immersed in hexadecane. The linewidths for $C_{11}$ and $C_3$ are the same within experimental error. These observations may be explained by the fact that $RePhen(CO)_3Cl$ is not soluble in hexadecane, and the solvent−headgroup interaction is not as great as in the case of DMF.

**B. 2D-IR Vibrational Echo Spectroscopy.** *1. Dynamics of Monolayer−Air Interfaces.* Figure 2 displays typical 2D IR spectra of the symmetric CO stretching mode of $RePhen(CO)_3Cl$ at the monolayer−air interface for $C_{11}$ (A) and $C_3$ (B) monolayers at a short and a long $T_w$. The 0−1 transition 2D vibrational bands are the red peaks. Below them, a portion of the 1−2 peaks (blue) can also be seen. The dashed line in the top left panel is the diagonal. At short time ($T_w$ = 0.5 ps), the spectra are elongated along the diagonal because there has not been sufficient time for the structural fluctuations to sample all possible structural configurations that give rise to the inhomogeneously broadened absorption lines. As $T_w$ becomes longer, more and more structures are sampled, and the spectra become more symmetrical about the diagonal. This is evident in the $T_w$ = 40 ps panels. At 40 ps, the spectrum of the $C_{11}$ system (top panels) is almost round, which shows that spectral diffusion is almost complete, i.e., almost all structural configurations have been sampled. At 40 ps, the spectrum of the $C_3$ system (bottom panels) is still somewhat elongated, although much less so than at short time. Thus for the $C_3$ system at 40 ps, spectral diffusion is not nearly as complete as it is for the $C_{11}$ system.


dx.doi.org/10.1021/jp410683h | J. Phys. Chem. C 2014, 118, 523−532

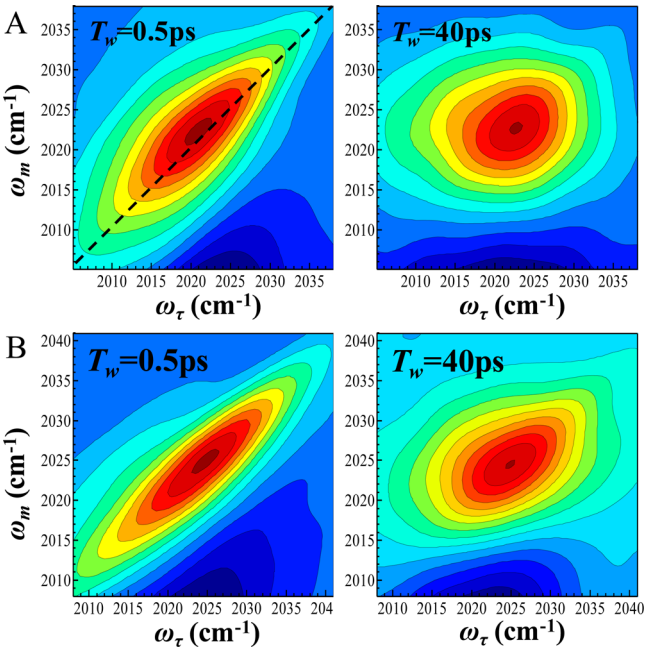


**Figure 2.** 2D IR spectra of the of CO symmetric stretching mode of RePhen(CO)$_3$Cl immobilized on monolayer/air interfaces for $C_{11}$ (A) and $C_3$ (B) alkyl chain lengths. The dashed line in the upper left panel is the diagonal. For longer waiting time, $T_w$, the band shapes become more symmetric (less elongated along the diagonal), demonstrating the existence of the spectral diffusion.

The time dependences of the band shapes were quantitatively analyzed by the CLS method.[56,57] CLS decays for the $C_{11}$ and $C_3$ systems are shown in Figure 3 (points). Curves such as

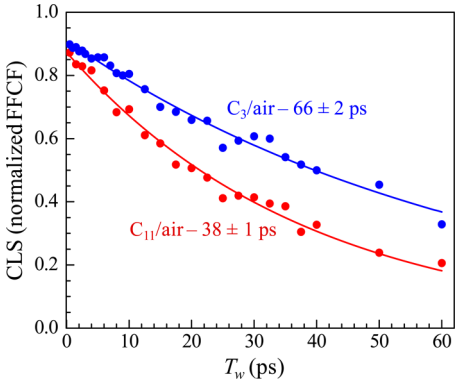


**Figure 3.** The averaged CLS decays for the monolayer/air interfaces for the $C_{11}$ (red points) and the $C_3$ (blue points) linking chain lengths. The solid curves are single exponential fits to the data.

those shown in Figure 3 were taken for a number of separately prepared samples. The data in Figure 3 are the averages of CLS decays obtained from all $C_{11}$ or $C_3$ monolayers studied. Since the CLS is directly proportional to the FFCF, the CLS decay time constant is equivalent to the spectral diffusion time constant ($\tau_1$ in Table 2). The CLS decays for both the $C_{11}$ monolayer–air and the $C_3$ monolayer–air interfaces were fit well with single exponentials with negligible offsets from zero (solid curves). The spectral diffusion time constant for the $C_3$ monolayer (66 ± 2 ps) was significantly slower than the $C_{11}$ monolayer (38 ± 1 ps). In a prior study it was implied that the $C_3$ dynamics were slower than the $C_{11}$ dynamics, but the data could only be taken out to 10 ps, and therefore the difference was not conclusive.[49] Here, with data collection to 60 ps and greatly improved data quality, it is clear that the spectral diffusion is substantially slower for $C_3$ chains compared to $C_{11}$ chains. The homogeneous line width extracted for the $C_3$ monolayer (1.8 cm$^{-1}$) is smaller than $C_{11}$ monolayer (2.3 cm$^{-1}$), while the frequency fluctuation amplitude for the spectral diffusion is larger for $C_3$ monolayer (7.8 cm$^{-1}$ for $C_3$ and 7.1 cm$^{-1}$ for $C_{11}$, see Table 2).

**Table 2. FFCF Parameters for the Symmetric CO Stretching Mode of RePhen(CO)$_3$Cl for Monolayer–Air Interfaces**

| sample | Γ (cm$^{-1}$) | $\Delta_1$ (cm$^{-1}$) | $\tau_1$ (ps) |
|---|---|---|---|
| $C_{11}$ | 2.3 | 7.1 | 38 ± 1 |
| $C_3$ | 1.8 | 7.8 | 66 ± 2 |

As these samples are monolayers in air, there is no solvent dynamics to contribute to the spectral diffusion. The RePhen(CO)$_3$Cl headgroup is rigid, with the lowest frequency vibrational modes all above ∼100 cm$^{-1}$. Thus, internal structural evolution of the headgroup would not contribute to the spectral diffusion. Therefore, spectral diffusion must be caused by motions associated with the monolayer itself. The linkage between the headgroup and the alkyl chains is the same for $C_{11}$ and $C_3$ chain length samples. Therefore, it is reasonable to attribute the origin of the differences in the spectral diffusion to the structural evolution of tethering alkyl chains, with a possible contribution from the underlying network that anchors the chains to the $SiO_2$ surface.

The fact that $C_3$ monolayers produce slower spectral diffusion than the $C_{11}$ monolayers supports the idea that motions of the alkyl chains with the attached linkage and headgroup result in the spectral diffusion (fluctuations in the structure of the monolayer). The $C_{11}$ chains are longer with more methylene groups, giving rise to more degrees of freedom than the $C_3$ chains. The additional degrees of freedom of the $C_{11}$ monolayers may produce more rapid sampling of configurations than the $C_3$ monolayers. Another factor was brought up in the discussion of Figure 1A,B. The literature indicates that the $C_3$ monolayers should have more "defects" than the $C_{11}$ monolayers, although the nature of the defects is not explicated.[61,62,65] The FT-IR spectra of the $C_3$ monolayers (Figure 1B) show different peak positions and much more variations compared with the case of $C_{11}$ monolayers (Figure 1A). All of this suggests that the $C_3$ and the $C_{11}$ monolayer structures are different, and this difference results in slower dynamics for the shorter chain length monolayer.

*2. Dynamics of Monolayer Exposed to Solvent Interfaces.* The dynamics of the $C_{11}$ and $C_3$ monolayers with the RePhen(CO)$_3$Cl headgroup IR probe were investigated in two solvents, DMF and hexadecane. DMF is a good solvent for the headgroup but is totally immiscible with alkanes. By contrast, RePhen(CO)$_3$Cl does not dissolve in hexadecane but hexadecane is miscible with alkyl chains.

Figure 4 displays the CLS decays for the $C_{11}$ and $C_3$ monolayers in DMF (points). Again, the CLS decays were obtained by averaging independent runs on three different samples for each type of monolayer. The decays are clearly biexponential, in contrast to the spectral diffusion dynamics of these same monolayers in air (see Figure 3). The FFCF parameters are given in Tables 3 and 4. As can be seen in Table 3, the homogeneous linewidths (Γ), the components of the inhomogeneous line width ($\Delta_1$ and $\Delta_2$), and the total


dx.doi.org/10.1021/jp410683h | J. Phys. Chem. C 2014, 118, 523–532

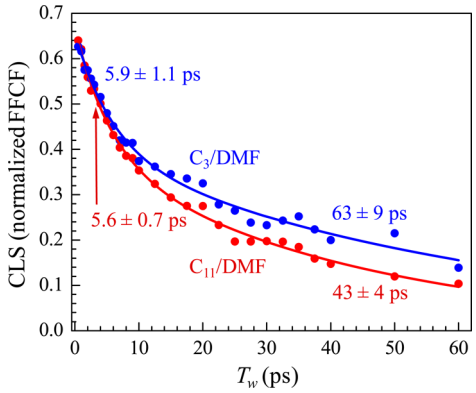


**Figure 4.** The averaged CLS decays for the monolayer/DMF interfaces for $C_{11}$ (red points) and $C_3$ (blue points) linking chain lengths. Both of the decays are fit with biexponential forms (solid curves). The faster decaying components for each data set are indistinguishable within error. The time constants for the slower decaying components are in good agreement with those on the monolayer/air interfaces, indicating that the slower components correspond to the tethering alkyl chain dynamics. The fast components are assigned to interfacial DMF dynamics.

inhomogeneous line width ($\Delta_{tot}$) are all essentially the same for the two chain length monolayers in contact with DMF. This is in agreement with the fact that the FT-IR spectra for $C_3$/DMF and $C_{11}$/DMF interfaces are almost the same. Within experimental error, the fast components of both the $C_{11}$ and $C_3$ monolayers are the same. In addition, the slow components are the same as they were in air within experimental error (see Tables 2 and 3).

The biexponential CLS decays for the monolayer–DMF interfaces can be understood in the following manner. Because the slowly decaying component for each chain length has essentially the same time constant as the time constants of monolayer–air interfaces, it is reasonable to assign this component to the structural dynamics associated with the alkyl chain/linker/headgroup in the manner discussed above for the samples in air. Apparently, DMF has little impact on the internal dynamics of the monolayers, which is reasonable given its total immiscibility with alkanes. It is unlikely that a substantial amount of DMF would be found in the alkyl regions of the monolayers.

In contrast to the alkyl chain regions of the monolayers, it is clear that DMF interacts with the head groups given the changes in the FT-IR spectra (Figure 1 and Table 1). The fast decaying component (~5.8 ps), can be attributed to the interfacial DMF dynamics. This conclusion is supported by the fact that the fast components of the FFCFs for the two types of monolayers are the same, while the slow components differ and are essentially the same as those measured for the monolayer–air interfaces. Thus, the interfacial solvent dynamics are monitored through the IR probe immobilized on the monolayer. This reporting on the interfacial solvent dynamics is equivalent to an IR probe in a bulk liquid reporting on the dynamic of the liquid, e.g., the OD stretch of HOD in bulk $H_2O$.[28,29] The IR probe experiences the interfacial DMF solvents structural configurations rather quickly, ~5.8 ps, and then it slowly samples the variety of internal configurations of the monolayers, 43 ps for $C_{11}$ monolayers and 63 ps for $C_3$ monolayers.

Table 3 also gives the FFCF for the RePhen(CO)$_3$Cl headgroup in bulk DMF solution.[50] In bulk DMF solution, the FFCF decays as a biexponential with the time constants of 1.8 and 11.9 ps. The homogeneous line width is slightly larger, and the total inhomogeneous contribution to the absorption spectrum is substantially smaller. Dynamics of molecules at interfaces in general will not be the same as their dynamics in bulk solution. For example, the orientational relaxation time of water at the interface of AOT reverse micelles is 18 ps in contrast to bulk water's 2.6 ps orientational relaxation time.[66,67] It is possible that in DMF the fast component of the interfacial dynamics (~5.8 ps) reflects a slowing of the fast component of RePhen(CO)$_3$Cl in bulk DMF (1.8 ps), and the slow component is absent at the interface. It is also possible that the slow component becomes substantially slower, and is merged with the slow decay component that arises from the monolayer structural fluctuation.

Figure 5 shows the CLS decays for symmetric CO stretch of the RePhen(CO)$_3$Cl headgroup on $C_{11}$ and $C_3$ monolayers in hexadecane (points). Figure 1 and Table 1 show that the influence of nonpolar hexadecane on the FT-IR spectra of the IR probe on $C_{11}$ and $C_3$ monolayers is not as great as that of polar DMF. In hexadecane, for the $C_{11}$ system, the peak position is essentially unchanged, and for the $C_3$ system, the peak is shifted slightly to the red. Nonetheless, immersion in

**Table 4. FFCF Parameters for the Symmetric CO Stretching Mode of RePhen(CO)$_3$Cl for Monolayer–Hexadecane Interfaces[a]**

| sample | $\Gamma$ ($cm^{-1}$) | $\Delta_1$ ($cm^{-1}$)[b] | $\tau_1$ (ps)[b] | $\Delta_2$ ($cm^{-1}$) | $\tau_2$ (ps) | $\Delta_{tot}$ ($cm^{-1}$) |
|---|---|---|---|---|---|---|
| $C_{11}$/ hexadecane | 1.9 | 3.2 | 13 ± 4 | 4.2 | 48 ± 9 | 5.3 |
| $C_3$/ hexadecane | 2.0 | 3.2 | 13 ± 4 | 4.7 | 79 ± 24 | 5.9 |

[a]$\Gamma$ - homogeneous line width (full-width-half-maximum). $\Delta_i$ are the standard deviations of the frequency fluctuation amplitudes associated with the time constant, $\tau_i$. $\Delta_{tot}$ is the total inhomogeneous width standard deviation, which is the square root of the sum of the squares of the $\Delta_i$. The full width at half-maximum is obtained by multiplying by 2.35. [b]Global fit.

**Table 3. FFCF Parameters for the Symmetric CO Stretching Mode of RePhen(CO)$_3$Cl for Monolayer–DMF Interfaces and the RePhen(CO)$_3$Cl Head Group in Bulk DMF[a]**

| sample | $\Gamma$ ($cm^{-1}$) | $\Delta_1$ ($cm^{-1}$) | $\tau_1$ (ps) | $\Delta_2$ ($cm^{-1}$) | $\tau_2$ (ps) | $\Delta_{tot}$ ($cm^{-1}$) |
|---|---|---|---|---|---|---|
| $C_{11}$/DMF | 3.0 | 2.9 | 5.6 ± 0.7 | 3.3 | 43 ± 4 | 4.4 |
| $C_3$/DMF | 3.3 | 2.7 | 5.9 ± 1.1 | 3.4 | 63 ± 9 | 4.3 |
| RePhen(CO)$_3$Cl in bulk DMF | 3.95 | 1.88 | 1.8 ± 0.2 | 1.30 | 11.9 ± 1.3 | 2.29 |

[a]$\Gamma$ - homogeneous line width (full-width-half-maximum). $\Delta_i$ are the standard deviations of the frequency fluctuation amplitudes associated with the time constant, $\tau_i$. $\Delta_{tot}$ is the total inhomogeneous width standard deviation, which is square root of the sum of the squares of the $\Delta_i$. The full width at half-maximum is obtained by multiplying by 2.35.


dx.doi.org/10.1021/jp410683h | J. Phys. Chem. C 2014, 118, 523–532

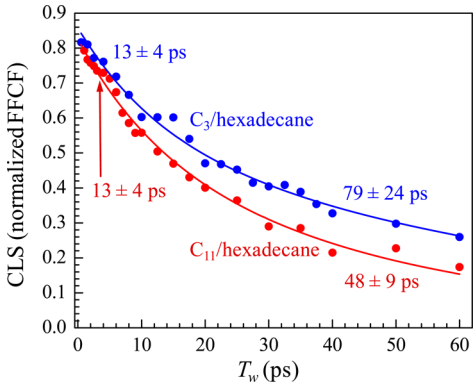


**Figure 5.** The averaged CLS decays for the monolayer/hexadecane interfaces for the $C_{11}$ (red points) and $C_3$ (blue points) linking chain lengths. Both data sets are fit with biexponential decays (solid curves).

hexadecane has a significant effect on the structural dynamics of the system.

Attempts to fit the CLS data shown in Figure 5 with single exponential decays gave poor fits. However, when the CLS decays on the monolayer−hexadecane interfaces were fit with biexponentials, large standard deviations in fitting parameters appeared, making it hard to accurately determine the dynamical constants. To obtain the dynamical constants, we draw on the results of the fits for the samples immersed in DMF (Figure 4), which show that the fast components of the decays are the same for the $C_{11}$ and $C_3$ monolayers within experimental error. For the samples in hexadecane, we assume that the decays are biexponentials, and time constant and amplitude of the faster decaying components are the same for the $C_{11}$ and $C_3$ systems. We performed a global fit to the two decays shown in Figure 5 with this assumption. Akaike Information Criterion (AIC),[68] which is a method that compares fitting models, was employed to test the most appropriate fitting function. The AIC method accounts for the number of fitting parameters in selecting between models. The statistical analysis demonstrates that when two independent single exponential fits are compared to biexponential fits with the constraints, the biexponential fits are overwhelmingly more likely to be the correct fitting model, even though there are more fitting parameters. The resulting fits are the solid curves in Figure 5.

In the global biexponential fits, the shared faster decay time constant,13 ± 4 ps, which probably originates from interfacial hexadecane dynamics, is significantly faster than the slower time constants, 48 ± 9 ps for $C_{11}$; 79 ± 24 ps for $C_3$. The slower time constants are within their relatively large error bars of the time constants found for the same samples in air, 38 ± 1 ps and 68 ± 2 ps, respectively. These slower time constants arise from the structural dynamics of the monolayers. We cannot compare the interfacial hexadecane solvent dynamics to those in the bulk solution as the IR probe, $RePhen(CO)_3Cl$, is insoluble in hexadecane.

**C. Polarization Selective Heterodyne Detected Transient Grating Experiments.** The polarization selected HDTG signals measured with ⟨*XXXX*⟩ polarizations and ⟨*XXYY*⟩ polarizations for $C_{11}$ monolayer−air interface are shown in Figure 6A. The experimental correction factor, *f*, discussed in Section II.C has been absorbed into $I_{XXXX}$. Therefore, Figure 6A shows $I_{XXXX}$ and $I_{XXYY}$ with the correct relative amplitudes. It is clear that the ⟨*XXXX*⟩ signal has a

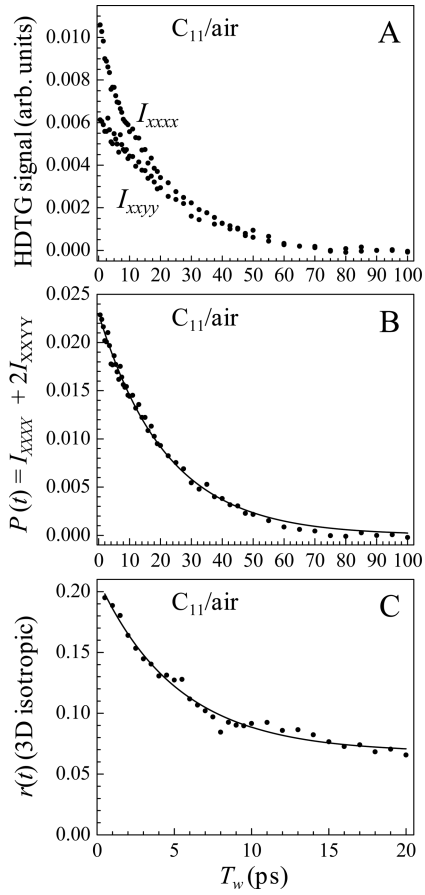


**Figure 6.** (A) TThe polarization selective HDTG signals for the CO symmetric stretching mode of $RePhen(CO)_3Cl$ on the $C_{11}$/air interface with ⟨*XXXX*⟩ and ⟨*XXYY*⟩ polarizations. The steeper decay observed for the ⟨*XXXX*⟩ polarization shows that there is at least some orientational relaxation of the $RePhen(CO)_3Cl$ IR probe. (B) Population relaxation of the CO symmetric stretching mode of $RePhen(CO)_3Cl$ on the $C_{11}$/air interface (points) from the data in A. The solid curve is a single exponential fit to the data with a time constant of 21.8 ps. Although the sample is a monolayer, usable data could be obtained to ∼5 lifetimes. (C) The anisotropy decay for the $C_{11}$/air interface calculated as $r(t) = (I_{XXXX} - I_{YYXX})/(I_{XXXX} + 2I_{YYXX})$ (see text) from the data in A (points). The solid curve is an exponential fit with an offset, showing that there is angular sampling of a limited range of angles, a cone of angles, and that the axis of the cone is tilted from the surface normal.

steeper decay than the ⟨*XXYY*⟩ signal, which demonstrates that there is orientational relaxation occurring.

$P(t)$ and $r(t)$ (defined in eqs 3 and 4) calculated from $I_{XXXX}$ and $I_{XXYY}$ in Figure 6A are shown in Figure 6B and Figure 6C. $P(t)$ shown in Figure 6B was fit well to single exponential decay with the decaying time constant $T_1$ = 21.8 ps. Due to high sensitivity of HDTG, high-quality anisotropy data, $r(t)$, were obtained as shown in Figure 6C, in spite of the fact that the signal is from a single layer of molecule. $r(t)$ can be fit well with single exponential ($\tau_c$ = 5.2 ps) plus significant plateau ($r(\infty)$ = 0.07). The plateau in the anisotropy indicates that there is restriction in transition dipole's motion that is typically interpreted with the "wobbling-in-a-cone" model.[51−54] Fitting parameters of $P(t)$ and $r(t)$ for $C_{11}$ and $C_3$ samples with and without solvents are listed in Table 5 and 6.

For the case in which the transition dipoles are randomly oriented in a sample, $T_1$ is the vibrational lifetime, and $\tau_c$ is the


dx.doi.org/10.1021/jp410683h | J. Phys. Chem. C 2014, 118, 523−532

Table 5. Vibrational Lifetimes, $T_1$

| sample | $T_1$(ps) |
|---|---|
| $C_{11}$/air | 21.8 ± 0.4 |
| $C_3$/air | 19.5 ± 0.4 |
| $C_{11}$/DMF | 20.3 ± 0.4 |
| $C_3$/DMF | 18.1 ± 0.4 |
| $C_{11}$/hexadecane | 20.4 ± 0.4 |
| $C_3$/hexadecane | 19.2 ± 0.4 |

Table 6. Orientational Relaxation Time Constants $\tau_c$ and Offsets in Anisotropy $r(t)$

| sample | $\tau_c$(ps) | $r(\infty)$ |
|---|---|---|
| $C_{11}$/air | 5.2 ± 1.1 | 0.07 ± 0.01 |
| $C_3$/air | 3.9 ± 1.3 | 0.06 ± 0.01 |
| $C_{11}$/DMF | 6.4 ± 0.9 | 0.09 ± 0.01 |
| $C_3$/DMF | 9.9 ± 5.0 | 0.03 ± 0.03 |
| $C_{11}$/hexadecane | 8.7 ± 2.4 | 0.05 ± 0.02 |
| $C_3$/hexadecane | 7.6 ± 3.2 | 0.08 ± 0.02 |

orientational relaxation time constant.[58,59] An isotropic distribution is not appropriate for transition dipoles in an organic monolayer since the out-of-plane direction of the transition dipoles is restricted. However, for the reasons described below, the qualitative comparisons of $\tau_c$ and $r(\infty)$ in Tables 5 and 6 are nonetheless useful for these samples.

In the case where out-of-plane motions of the transition dipoles are completely frozen, it is known that orientational correlation function is proportional to $r'(t) = (I_{XXXX} - I_{XXYY})/(I_{XXXX} + I_{XXYY})$, while population decay is proportional to $P'(t) = I_{XXXX} + I_{XXYY}$.[69] When $P'(t)$ and $r'(t)$ were calculated instead of $P(t)$ and $r(t)$ for all the samples in Tables 5 and 6, $T_1$ and $\tau_c$ obtained from $P'(t)$and $r'(t)$ were almost the same as those listed in Tables 5 and 6 within the error. The actual monolayer's orientational motions will be between the two cases in which all dipole orientations can be sampled (isotropic) and the out-of-plane motions are frozen. Since the two forms for analyzing the population and orientational decays gave very similar results, $T_1$ and $\tau_c$ can be regarded as essentially the vibrational lifetime and the decay time constant for orientational correlation function.

In Table 5, it can be seen that vibrational lifetimes are not drastically affected by linker's chain length or the presence of solvent. This similarity of all of the vibrational lifetimes suggests that vibrational relaxation is dominated by coupling to the intramolecular modes of the headgroup, with both the structure of the monolayer and the solvent playing a minor role.

The orientational relaxation time constants $\tau_c$ in Table 6 implies certain variations depending on chain length and the presence of solvent. It is interesting that once the monolayers are immersed in a solvent, $\tau_c$ tends to slow down. One possible explanation is that the orientational diffusion constant $D$ decreased due to molecular level "friction" between the headgroup and interfacial solvent molecules. There is another possibility that the wobbling-cone angle $\theta_C$ is affected by immersing the monolayer in solvent. It is well-known that $\tau_c$ increases as cone angle $\theta_C$ decreases even if the $D$ is unchanged.[51]

To distinguish these two possibilities, the cone angle $\theta_C$ must be known. In systems in which the transition dipoles are randomly oriented, $\theta_C$ can be obtained from the plateau level in anisotropy, $r(\infty)$. However, the same strategy cannot be employed for a two-dimensional monolayer since the transition dipoles are not randomly oriented in the out-of-plane direction and the cone axis may not be normal to the plane. To our knowledge, there is no theoretical framework describing how to extract detailed wobbling-in-a-cone parameters from depolarization experiments on molecules bound to two-dimensional surfaces. The necessary theoretical development is in progress. Based on the primary theoretical results, the significant plateau in the anisotropy indicates that the primary axis of the cone must be tilted away from the normal axis of the surface, which is in agreement with our previous result that the average tilt angle of transition dipoles in the sample is ~60°.[49]

## IV. CONCLUDING REMARKS

The $C_{11}$ monolayer and $C_3$ monolayer functionalized with the headgroup, RePhen$(CO)_3$Cl, which serves as the IR probe, have distinctively different dynamics in air as measured with ultrafast 2D IR vibrational echo experiments. For the monolayer/air interfaces, both the $C_{11}$ and $C_3$ monolayers have FFCFs decays (spectral diffusion) that are single exponentials with time constants of 38 ± 1 ps and 66 ± 2 ps, respectively. Thus, the observed dynamics of the surface bound species that comprise the monolayers depend on the chair length. This chain length dependence of the observed time constants indicates that the spectral diffusion is induced by the structural dynamics involving the tethering alkyl chains.

When the monolayers were immersed in DMF, the FFCF decays become biexponential. The amplitude and the spectral diffusion time constants for the faster decay component of the two chain length samples are the same within experimental error, ~5.8 ps, which suggests that this decay component originates from the dynamics of DMF at the interface. The slower components, 43 ± 4 ps for $C_{11}$ and 63 ± 9 ps and $C_3$ monolayer, are within experimental error of the same spectral diffusion time constants as the corresponding monolayer−air interfaces. These slower components are assigned to the monolayers' structural motions that are influenced by the chain length. These results suggest that exposing the interface to DMF does not change the structural dynamics internal to the monolayer. The FFCF decays for the monolayer/hexadecane interfaces were interpreted in the same manner as monolayer/DMF interfaces, indicating that the interfacial hexadecane dynamics give rise to the spectral diffusion time constant of 13 ± 4 ps. The IR probes at the monolayer−solvent interface provide information on solvent molecular dynamics at the interface. This approach for addressing interfacial solvent dynamics is, in principle, applicable to any solvent, regardless of the solubility of the IR probe in solvent of interest.

The first measurements of interfacial orientational dynamics using IR polarization selective heterodyne detected transient grating spectroscopy were presented. These measurements also give the vibrational lifetimes. The heterodyne detected transient grating experiment provides the necessary sensitivity to observe a monolayer, which cannot be done with a far less sensitive IR pump−probe experiment. It was possible to measure the population relaxation out to five vibrational lifetimes even though the measurements were made on monolayers. The results of the orientational relaxation measurements demonstrate that there is limited orientational relaxation, which is referred to as wobbling-in-a-cone. The orientational dynamics occur on a 5 to 10 ps time scale. However, full interpretation of the wobbling motion requires the extension of the isotropic 3D wobbling-in-a-cone theory[51,52] to that of a surface system with


dx.doi.org/10.1021/jp410683h | J. Phys. Chem. C 2014, 118, 523−532

tilted cones. The development of the theory will allow us to fully characterize the wobbling motions of the organic monolayers based on polarization selective HDTG experiments.

## AUTHOR INFORMATION


### Corresponding Author

*E-mail: fayer@stanford.edu.


### Notes

The authors declare no competing financial interest.

## ACKNOWLEDGMENTS

This material is based upon work supported by the Air Force Office of Scientific Research Grant FA9550-12-1-0050. Jun Nishida also thanks the Stanford Graduate Fellowship programs for a fellowship.

## REFERENCES


(1) Terry, T. J.; Stack, T. D. P. Covalent Heterogenization of a Discrete Mn (II) Bis-Phen Complex by a Metal-Template/Metal-Exchange Method: An Epoxidation Catalyst with Enhanced Reactivity. *J. Am. Chem. Soc.* **2008**, *130*, 4945−4953.

(2) Minakata, S.; Komatsu, M. Organic Reactions on Silica in Water. *Chem. Rev.* **2008**, *109*, 711−724.

(3) Fraile, J. M.; García, J. I.; Herrerías, C. I.; Mayoral, J. A.; Pires, E. Enantioselective Catalysis with Chiral Complexes Immobilized on Nanostructured Supports. *Chem. Soc. Rev.* **2009**, *38*, 695−706.

(4) Thomas, J. M.; Raja, R. Exploiting Nanospace for Asymmetric Catalysis: Confinement of Immobilized, Single-Site Chiral Catalysts Enhances Enantioselectivity. *Acc. Chem. Res.* **2008**, *41*, 708−720.

(5) Yamada, H.; Imahori, H.; Nishimura, Y.; Yamazaki, I.; Ahn, T. K.; Kim, S. K.; Kim, D.; Fukuzumi, S. Photovoltaic Properties of Self-Assembled Monolayers of Porphyrins and Porphyrin-Fullerene Dyads on ITO and Gold Surfaces. *J. Am. Chem. Soc.* **2003**, *125*, 9129−9139.

(6) Crooks, R. M.; Ricco, A. J. New Organic Materials Suitable for Use in Chemical Sensor Arrays. *Acc. Chem. Res.* **1998**, *31*, 219−227.

(7) Kepley, L. J.; Crooks, R. M.; Ricco, A. J. Selective Surface Acoustic Wave-Based Organophosphonate Chemical Sensor Employing a Self-Assembled Composite Monolayer: A New Paradigm for Sensor Design. *Anal. Chem.* **1992**, *64*, 3191−3193.

(8) Liu, G.; Paddon-Row, M. N.; Gooding, J. J. Protein Modulation of Electrochemical Signals: Application to Immunobiosensing. *Chem. Commun.* **2008**, *33*, 3870−3872.

(9) Ciampi, S.; James, M.; Le Saux, G.; Gaus, K.; Gooding, J. J. Electrochemical "Switching" of Si (100) Modular Assemblies. *J. Am. Chem. Soc.* **2011**, *134*, 844−847.

(10) Hamoudi, H.; Dablemont, C.; Esaulov, V. A. Disorder, Solvent Effects and Substitutional Self-Assembly of Alkane Dithiols from Alkane Thiol Sams. *Surf. Sci.* **2011**, *605*, 116−120.

(11) Duwez, A. S.; Yu, L. M.; Riga, J.; Pireaux, J. J.; Delhalle, J. Molecular Structure and Surface Order in Monolayers of Alkanethiols Evidenced by Hreels. *Thin Solid Films* **1998**, *327*−*329*, 156−160.

(12) Bratlie, K. M.; Komvopoulos, K.; Somorjai, G. A. Sum Frequency Generation Vibrational Spectroscopy of Pyridine Hydrogenation on Platinum Nanoparticles. *J. Phys. Chem. C* **2008**, *112*, 11865−11868.

(13) Devadoss, A.; Chidsey, C. E. D. Azide-Modified Graphitic Surfaces for Covalent Attachment of Alkyne-Terminated Molecules by "Click" Chemistry. *J. Am. Chem. Soc.* **2007**, *129*, 5370−5371.

(14) Banga, R.; Yarwood, J.; Morgan, A. M.; Evans, B.; Kells, J. Ftir and AFM Studies of the Kinetics and Self-Assembly of Alkyltrichlorosilanes and (Perfluoroalkyl)Trichlorosilanes onto Glass and Silicon. *Langmuir* **1995**, *11*, 4393−4399.

(15) Meyer, E.; Overney, R.; Lüthi, R.; Brodbeck, D.; Howald, L.; Frommer, J.; Güntherodt, H. J.; Wolter, O.; Fujihira, M.; Takano, H.; Gotoh, Y. Friction Force Microscopy of Mixed Langmuir-Blodgett Films. *Thin Solid Films* **1992**, *220*, 132−137.

(16) Florio, G. M.; Werblowsky, T. L.; Ilan, B.; Müller, T.; Berne, B. J.; Flynn, G. W. Chain-Length Effects on the Self-Assembly of Short 1-Bromoalkane and N-Alkane Monolayers on Graphite. *J. Phys. Chem. C* **2008**, *112*, 18067−18075.

(17) Shen, Y. R.; Ostroverkhov, V. Sum-Frequency Vibrational Spectroscopy on Water Interfaces: Polar Orientation of Water Molecules at Interfaces. *Chem. Rev.* **2006**, *106*, 1140−1154.

(18) Yamaguchi, S.; Tahara, T. Heterodyne-Detected Electronic Sum Frequency Generation:"Up" Versus "Down" Alignment of Interfacial Molecules. *J. Chem. Phys.* **2008**, *129*, 101102.

(19) Zhuang, X.; Miranda, P. B.; Kim, D.; Shen, Y. R. Mapping Molecular Orientation and Conformation at Interfaces by Surface Nonlinear Optics. *Phys. Rev. B* **1999**, *59*, 12632.

(20) Chen, Z.; Shen, Y. R.; Somorjai, G. A. Studies of Polymer Surfaces by Sum Frequency Generation Vibrational Spectroscopy. *Annu. Rev. Phys. Chem.* **2002**, *53*, 437−465.

(21) Zimdars, D.; Dadap, J. I.; Eisenthal, K. B.; Heinz, T. F. Anisotropic Orientational Motion of Molecular Adsorbates at the Air-Water Interface. *J. Phys. Chem. B* **1999**, *103*, 3425−3433.

(22) Nguyen, K. T.; Shang, X.; Eisenthal, K. B. Molecular Rotation at Negatively Charged Surfactant/Aqueous Interfaces. *J. Phys. Chem. B* **2006**, *110*, 19788−19792.

(23) Shang, X.; Nguyen, K.; Rao, Y.; Eisenthal, K. B. In-Plane Molecular Rotational Dynamics at a Negatively Charged Surfactant/Aqueous Interface. *J. Phys. Chem. C* **2008**, *112*, 20375−20381.

(24) Hsieh, C. S.; Campen, R. K.; Verde, A. C. V.; Bolhuis, P.; Nienhuys, H. K.; Bonn, M. Ultrafast Reorientation of Dangling OH Groups at the Air-Water Interface Using Femtosecond Vibrational Spectroscopy. *Phys. Rev. Lett.* **2011**, *107*, 116102.

(25) Gengeliczki, Z.; Rosenfeld, D. E.; Fayer, M. D. Theory of Interfacial Orientational Relaxation Spectroscopic Observables. *J. Chem. Phys.* **2010**, *132*, 244703−244703.

(26) Fayer, M. D.; Moilanen, D. E.; Wong, D.; Rosenfeld, D. E.; Fenn, E. E.; Park, S. Water Dynamics in Salt Solutions Studied with Ultrafast Two-Dimensional Infrared (2D IR) Vibrational Echo Spectroscopy. *Acc. Chem. Res.* **2009**, *42*, 1210−1219.

(27) Moilanen, D. E.; Wong, D.; Rosenfeld, D. E.; Fenn, E. E.; Fayer, M. D. Ion-Water Hydrogen-Bond Switching Observed with 2D IR Vibrational Echo Chemical Exchange Spectroscopy. *Proc. Nat. Acad. Sci. U.S.A.* **2009**, *106*, 375−380.

(28) Asbury, J. B.; Steinel, T.; Kwak, K.; Corcelli, S. A.; Lawrence, C. P.; Skinner, J. L.; Fayer, M. D. Dynamics of Water Probed with Vibrational Echo Correlation Spectroscopy. *J. Chem. Phys.* **2004**, *121*, 12431−12446.

(29) Asbury, J. B.; Steinel, T.; Stromberg, C.; Corcelli, S. A.; Lawrence, C. P.; Skinner, J. L.; Fayer, M. D. Water Dynamics: Vibrational Echo Correlation Spectroscopy and Comparison to Molecular Dynamics Simulations. *J. Phys. Chem. A* **2004**, *108*, 1107−1119.

(30) Loparo, J. J.; Roberts, S. T.; Tokmakoff, A. Multidimensional Infrared Spectroscopy of Water. II. Hydrogen Bond Switching Dynamics. *J. Chem. Phys.* **2006**, *125*, 194522−194522.

(31) Wong, D. B.; Giammanco, C. H.; Fenn, E. E.; Fayer, M. D. Dynamics of Isolated Water Molecules in a Sea of Ions in a Room Temperature Ionic Liquid. *J. Phys. Chem. B* **2013**, *117*, 623−635.

(32) Giammanco, C. H.; Wong, D. B.; Fayer, M. D. Water Dynamics in Divalent and Monovalent Concentrated Salt Solutions. *J. Phys. Chem. B* **2012**, *116*, 13781−13792.

(33) Zheng, J. R.; Kwak, K.; Asbury, J.; Chen, X.; Piletic, I. R.; Fayer, M. D. Ultrafast Dynamics of Solute-Solvent Complexation Observed at Thermal Equilibrium in Real Time. *Science* **2005**, *309*, 1338−1343.

(34) Zheng, J. R.; Kwak, K.; Chen, X.; Asbury, J. B.; Fayer, M. D. Formation and Dissociation of Intra-Intermolecular Hydrogen-Bonded Solute-Solvent Complexes: Chemical Exchange Two-Dimensional Infrared Vibrational Echo Spectroscopy. *J. Am. Chem. Soc.* **2006**, *128*, 2977−2987.

(35) Kwak, K.; Rosenfeld, D. E.; Chung, J. K.; Fayer, M. D. Solute-Solvent Complex Switching Dynamics of Chloroform between

Acetone and Dimethylsulfoxide-Two-Dimensional IR Chemical Exchange Spectroscopy. *J. Phys. Chem. B* **2008**, *112*, 13906−13915.
(36) Kim, Y. S.; Hochstrasser, R. M. Chemical Exchange 2D IR of Hydrogen-Bond Making and Breaking. *Proc. Natl. Acad. Sci. U.S.A.* **2005**, *102*, 11185−11190.
(37) Ishikawa, H.; Kwak, K.; Chung, J. K.; Kim, S.; Fayer, M. D. Direct Observation of Fast Protein Conformational Switching. *Proc. Nat. Acad. Sci. U.S.A.* **2008**, *105*, 8619−8624.
(38) Finkelstein, I. J.; Ishikawa, H.; Kim, S.; Massari, A. M.; Fayer, M. D. Substrate Binding and Protein Conformational Dynamics Measured by 2D-IR Vibrational Echo Spectroscopy. *Proc. Nat. Acad. Sci. U.S.A.* **2007**, *104*, 2637−2642.
(39) Chung, J. K.; Thielges, M. C.; Bowman, S. E. J.; Bren, K. L.; Fayer, M. D. Temperature Dependent Equilibrium Native to Unfolded Protein Dynamics and Properties Observed with IR Absorption and 2D IR Vibrational Echo Experiments. *J. Am. Chem. Soc.* **2011**, *133*, 6681−6691.
(40) McGuire, J. A.; Shen, Y. R. Ultrafast Vibrational Dynamics at Water Interfaces. *Science* **2006**, *313*, 1945−1948.
(41) Guyot-Sionnest, P. Coherent Processes at Surfaces: Free-Induction Decay and Photon Echo of the Si-H Stretching Vibration for H/Si (111). *Phys. Rev. Lett.* **1991**, *66*, 1489−1492.
(42) Guyot-Sionnest, P.; Lin, P. H.; Hiller, E. M. Vibrational Dynamics of the Si−H Stretching Modes of the Si (100)/H: 2× 1 Surface. *J. Chem. Phys.* **1995**, *102*, 4269.
(43) Bredenbeck, J.; Ghosh, A.; Smits, M.; Bonn, M. Ultrafast Two Dimensional-Infrared Spectroscopy of a Molecular Monolayer. *J. Am. Chem. Soc.* **2008**, *130*, 2152−2153.
(44) Zhang, Z.; Piatkowski, L.; Bakker, H. J.; Bonn, M. Ultrafast Vibrational Energy Transfer at the Water/Air Interface Revealed by Two-Dimensional Surface Vibrational Spectroscopy. *Nature Chem.* **2011**, *3*, 888−893.
(45) Zhang, Z.; Piatkowski, L.; Bakker, H. J.; Bonn, M. Interfacial Water Structure Revealed by Ultrafast Two-Dimensional Surface Vibrational Spectroscopy. *J. Chem. Phys.* **2011**, *021101*, 104−106.
(46) Singh, P. C.; Nihonyanagi, S.; Yamaguchi, S.; Tahara, T. Ultrafast Vibrational Dynamics of Water at a Charged Interface Revealed by Two-Dimensional Heterodyne-Detected Vibrational Sum Frequency Generation. *J. Chem. Phys.* **2012**, *137*, 094706.
(47) Xiong, W.; Laaser, J. E.; Mehlenbacher, R. D.; Zanni, M. T. Adding a Dimension to the Infrared Spectra of Interfaces Using Heterodyne Detected 2D Sum-Frequency Generation (HD 2D SFG) Spectroscopy. *Proc. Nat. Acad. Sci. U.S.A.* **2011**, *108*, 20902−20907.
(48) Rosenfeld, D. E.; Gengeliczki, Z.; Smith, B. J.; Stack, T. D. P.; Fayer, M. D. Structural Dynamics of a Catalytic Monolayer Probed by Ultrafast 2D IR Vibrational Echoes. *Science* **2011**, *334*, 634−639.
(49) Rosenfeld, D. E.; Nishida, J.; Yan, C.; Gengeliczki, Z.; Smith, B. J.; Fayer, M. D. Dynamics of Functionalized Surface Molecular Monolayers Studied with Ultrafast Infrared Vibrational Spectroscopy. *J. Phys. Chem. C* **2012**, *116*, 23428−23440.
(50) Rosenfeld, D. E.; Nishida, J.; Yan, C.; Kumar, S. K.; Tamimi, A.; Fayer, M. D. Structural Dynamics at Monolayer−Liquid Interfaces Probed by 2D IR Spectroscopy. *J. Phys. Chem. C* **2013**, *117*, 1409−1420.
(51) Lipari, G.; Szabo, A. Effect of Librational Motion on Fluorescence Depolarization and Nuclear Magnetic-Resonance Relaxation in Macromolecules and Membranes. *Biophys. J.* **1980**, *30*, 489−506.
(52) Wang, C. C.; Pecora, R. Time-Correlation Functions for Restricted Rotational Diffusion. *J. Chem. Phys.* **1980**, *72*, 5333−5340.
(53) Tan, H. S.; Piletic, I. R.; Fayer, M. D. Orientational Dynamics of Water Confined on a Nanometer Length Scale in Reverse Micelles. *J. Chem. Phys.* **2005**, *122*, 174501.
(54) Piletic, I. R.; Moilanen, D. E.; Spry, D. B.; Levinger, N. E.; Fayer, M. D. Testing the Core/Shell Model of Nanoconfined Water in Reverse Micelles Using Linear and Nonlinear IR Spectroscopy. *J. Phys. Chem. A* **2006**, *110*, 4985−4999.
(55) Khalil, M.; Demirdoven, N.; Tokmakoff, A. Obtaining Absorptive Line Shapes in Two-Dimensional Infrared Vibrational Correlation Spectra. *Phys. Rev. Lett.* **2003**, *90*, 047401.
(56) Kwak, K.; Park, S.; Finkelstein, I. J.; Fayer, M. D. Frequency-Frequency Correlation Functions and Apodization in Two-Dimensional Infrared Vibrational Echo Spectroscopy: A New Approach. *J. Chem. Phys.* **2007**, *127*, 124503.
(57) Kwak, K.; Rosenfeld, D. E.; Fayer, M. D. Taking Apart the Two-Dimensional Infrared Vibrational Echo Spectra: More Information and Elimination of Distortions. *J. Chem. Phys.* **2008**, *128*, 204505.
(58) Tokmakoff, A. Orientational Correlation Functions and Polarization Selectivity for Nonlinear Spectroscopy of Isotropic Media. I. Third Order. *J. Chem. Phys.* **1996**, *105*, 1−12.
(59) Tao, T. Time-Dependent Fluorescence Depolarization and Brownian Rotational Diffusion Coefficients of Macromolecules. *Biopolymers* **1969**, *8*, 609−632.
(60) Ulman, A. Formation and Structure of Self-Assembled Monolayers. *Chem. Rev.* **1996**, *96*, 1533−1554.
(61) Brzoska, J. B.; Azouz, I. B.; Rondelez, F. Silanization of Solid Substrates: A Step toward Reproducibility. *Langmuir* **1994**, *10*, 4367−4373.
(62) Xiao, X.; Hu, J.; Charych, D. H.; Salmeron, M. Chain Length Dependence of the Frictional Properties of Alkylsilane Molecules Self-Assembled on Mica Studied by Atomic Force Microscopy. *Langmuir* **1996**, *12*, 235−237.
(63) Stevens, M. J. Thoughts on the Structure of Alkylsilane Monolayers. *Langmuir* **1999**, *15*, 2773−2778.
(64) Nakagawa, T.; Ogawa, K.; Kurumizawa, T. Atomic Force Microscope Images of Monolayers from Alkyltrichlorosilane on Mica Surfaces and Studies on an Anchoring Mechanism of Alkyltrichlorosilane Molecules to the Surface. *Langmuir* **1994**, *10*, 525−529.
(65) Parikh, A. N.; Allara, D. L.; Azouz, I. B.; Rondelez, F. An Intrinsic Relationship between Molecular Structure in Self-Assembled N-Alkylsiloxane Monolayers and Deposition Temperature. *J. Phys. Chem.* **1994**, *98*, 7577−7590.
(66) Moilanen, D. E.; Fenn, E. E.; Wong, D.; Fayer, M. D. Water Dynamics in Large and Small Reverse Micelles: From Two Ensembles to Collective Behavior. *J. Chem. Phys.* **2009**, *131*, 014704.
(67) Fayer, M. D.; Levinger, N. E. Analysis of Water in Confined Geometries and at Interfaces. *Ann. Rev. Analytical Chem.* **2010**, *3*, 89−107.
(68) Akaike, H. New Look at Statistical-Model Identification. *IEEE Trans. Autom. Contr.* **1974**, *AC19*, 716−723.
(69) Nienhuys, H.-K.; Bonn, M. Measuring Molecular Reorientation at Liquid Surfaces with Time-Resolved Sum-Frequency Spectroscopy: A Theoretical Framework. *J. Phys. Chem. B* **2009**, *113*, 7564−7573.